Speed-Adaptation Mechanism

Robotic Prostheses Can Actively Regulate Joint Torque

By Tommaso Lenzi, Levi J. Hargrove, and Jonathon W. Sensinger

© ISTOCKPHOTO.COM/TONISPAN

By 2050, an estimated 1.5 million people in the United States will be living with a major lower-limb amputation [1], a condition that causes severe disability, particularly for persons with transfemoral (above-knee) amputations. These individuals expend up to twice the metabolic effort to walk at half the speed [2] of able-bodied persons, and they experience a higher risk of falls and secondary pathological conditions, such as osteoarthritis, back pain, and depression [3].

Passive prostheses cannot fully replace the biomechanical function of intact legs during walking, as they are unable to provide biologically accurate torque at the joint level [4]. Persons with amputations must compensate for this deficiency by increasing their muscular effort on both the residual limb and contralateral leg [5]. However, these compensatory strategies result in kinetic and kinematic gait asymmetries that reduce gait efficiency and cause higher stress on the musculoskeletal system [5].

Digital Object Identifier 10.1109/MRA.2014.2360305
Date of publication: 19 December 2014

How a Robotic Prosthesis Can Help

Robotic prostheses can actively regulate joint torque to match the kinetics and kinematics of an intact leg during walking [6]–[9], possibly restoring physiological gait efficiency and stability. The joint torque demand is not fixed but is dependent on the walking speed [10]. In the stance phase (i.e., with the foot on the ground), the torque profiles change nonlinearly with the walking speed to properly support body weight against gravity and to propel the body mass (BM) forward [11], [12]. In the swing phase (i.e., with the foot off the ground), a progressively faster movement must be generated at increased walking speeds to ensure the timely placement of the

1070-9932/14©2014IEEE

foot in preparation for the subsequent heel strike, regardless of the initial swing conditions (i.e., joint torque, angle, and velocity) generated during the stance phase [13]. Mimicking the biomechanical function of intact legs, therefore, requires adaptive regulation of the prosthetic joints based on the walking speed.

The available controllers for powered transfemoral prostheses cannot generalize across different walking speeds. The implementation of impedance-inspired control [14] requires that the joint torque is defined as a parametric function of angle and velocity, with different stiffness, damping, and equilibrium angle values for each discrete phase of the gait cycle (usually five). To obtain biologically accurate torques, this approach requires an explicit, experimental tuning of all parameters at a specific walking speed [15]. However, at different walking speeds, the prosthesis does not perform optimally; it provides incorrect body support and propulsion in the stance phase and movement trajectory and duration in the swing phase. Most importantly, speed-dependent parameters require patient-specific tuning, as individuals use different gait cadences—and therefore different joint velocities—to walk at the same speed. The need for patient- and speed-specific tuning diminishes the ability of impedance-inspired control strategies to adapt to different walking speeds.

Effective speed adaptation has been achieved for ankle–foot prostheses using two different control approaches. Herr and Grabowski [6] proposed a biophysically based approach that imitates muscle reflexes, allowing the device to obtain inherent speed adaptability by changing the prosthesis torque output without directly measuring the walking speed or cadence. The method proposed in [16] relied instead on preprogrammed ankle-torque profiles, based on a continuous estimate of the gait cycle and an explicit measure of the gait pace. A nonlinear control approach has recently been proposed to address the speed-adaptability issue in the stance phase [17]–[19]. Although these control approaches could be extended to transfemoral prostheses during the stance phase, they do not address the need for speed adaptability during the swing phase, which is a fundamental issue for transfemoral prostheses.

In this article, we propose an alternative control strategy that imitates the basic speed-adaptation mechanism used by intact legs and allows the robotic leg to achieve biologically accurate biomechanics across different walking speeds, without the need for speed- or patient-specific tuning.

For able-bodied subjects, walking speed greatly affects joint torque demand during both the stance and swing phase [10], though different speed-adaptation mechanisms seem to be involved in these two gait phases. In the stance phase, a complex torque modulation takes place, resulting in an overall net energy increase that is proportional to the walking speed. This speed-adaptation mechanism is well described by the trend of quasistiffness [20], [21] (the derivative of the torque–angle relationship with respect to the angle during the execution of the gait cycle), which changes consistently as a function of walking speed [22]–[24], resulting in speed-specific torque–angle curves. In the swing phase, fairly invariant angle trajectories are observed across different walking speeds after time normalization. When the walking speed increases, the swing-phase duration decreases proportionally to the stride duration, maintaining an almost constant ratio between the stance- and swing-phase durations. As expected for a ballistic position task, the joint torques increase proportionally with the walking speed during the swing phase [25]. Based on these observations, for our proposed prosthesis controller, we propose to enforce quasistiffness profiles in the stance phase and ballistic position control in the swing phase.

By directly encoding the quasistiffness profiles of an intact leg in the stance controller, we eliminate the need to explicitly tune the stance-phase control parameters. Most importantly, biologically accurate torque–angle curves can be obtained for any walking speed by encoding a few speed-specific curves from able-bodied studies [22] and by interpolating among them based on measured walking speed. Moreover, quasistiffness profiles define desired torque solely as a function of the current angle. So we can enforce the desired torque–angle relationship independently from joint velocity, which differs for each subject while walking at the same speed, thus, avoiding the need for patient-specific tuning.

Quasistiffness profiles have been successfully used for optimizing spring placement in powered prosthesis design [8], [26]. The presence of passive elements improves the prosthesis efficiency by storing rather than dissipating energy in the negative work phases of the gait cycle. However, passive elements reduce the ability to modulate stiffness, resulting in reduced prosthesis control flexibility [27]. In this article, we extend the use of quasistiffness to achieve biologically accurate speed adaptation by rendering speed-specific, able-bodied quasistiffness through active control of motor torque.

In the swing phase, we exploit a minimum-jerk trajectory generator to obtain biologically accurate movement of the prosthesis joints across walking speeds and users. Using this approach, we can obtain a physiological swing movement trajectory and duration at each step without subject- or speed-specific tuning. In fact, the minimum-jerk trajectory generator can automatically take the starting swing angle and velocity at each step and smoothly drive the prosthesis through a biomechanically appropriate trajectory in the desired time, which we defined proportional to the stance phase duration, thus, generalizing across walking speeds and users. Due to their inherent speed invariance, quasistiffness in the stance phase and minimum jerk in the swing phase are ideal control variables to achieve speed adaptability in robotic transfemoral prostheses.

For this experiment, we implemented the proposed controllers on the second-generation Vanderbilt transfemoral prosthesis [28] (Figure 1). Prior to testing on amputee patients, an exhaustive characterization of stance-phase quasistiffness control and swing-phase position control was performed in an experienced able-bodied subject wearing a bypass adapter to walk on the same powered prosthesis. Three transfemoral amputee patients then tested the speed adaptability of the proposed controller. The patients walked on a treadmill while the walking speed was gradually increased from 0.5 m/s to their maximum

comfortable speed (Table 1). The same test was then repeated while patients used their prescribed passive prostheses. Experimental results show that regulating these few constraints (quasistiffness profiles in stance and minimum-jerk trajectory in swing) successfully restored physiological gait kinematics and kinetics (e.g., correct torque profiles, power generation, and gait symmetry) across different walking speeds.

Figure 1. The Vanderbilt transfemoral prosthesis (photo courtesy of Brian Kersey, Associated Press).

Table 1. The patient characteristics and highest comfortable speed on a treadmill.

Patient Number	Gender	Age (years)	Height (m)	Weight (kg)	Maximum Tested Speed (m/s)	Prescribed Knee	Prescribed Foot
1	M	30	1.86	86.2	1.40	KX06, Endolite	Elite blade Endolite
2	M	66	1.75	86.0	1.25	C-Leg Ottobock	1C60 Triton Ottobock
3	M	24	1.75	78.0	1.00	C-leg Ottobock	Elite 2 Ottobock

Controller Design

The proposed controller (see Figure 2 for a block diagram representation) comprises three stages that address the following issues: 1) gait-phase and walking-speed estimates, 2) planning of joint torques, and 3) attainment of desired torque at the prosthetic joints.

Finite-State Machine Implementation

The first stage of the controller estimates the state of the user and prosthesis. A finite-state machine, as shown in Figure 3, uses the outputs from an inertial measurement unit (IMU) and a ground reaction force (GRF) sensor to estimate whether the prosthesis is lifted off the ground (i.e., the GRF is lower than 5% of the patient's BM) or statically supporting the patient's weight (i.e., the GRF is greater than 5% of the BM). When a shank velocity greater than 10°/s is detected while the prosthetic foot is on the ground, the prosthesis enters into walking mode, which is divided into a stance phase and a swing phase. The stance phase is divided into three subphases: 1) early stance, 2) midstance, and 3) late stance—following the quasistiffness trends observed in an able-bodied subject, as shown in Figure 4 and discussed in the "Walking Controller" section. The ankle velocity and shank orientation regulate the transition between the three stance subphases. Early stance starts when the prosthesis contacts the ground and ends with the inversion of ankle movement from plantarflexion to dorsiflexion. The midstance phase is characterized by dorsiflexion of the ankle joint. When ankle movement is again inverted from dorsiflexion to plantarflexion with a shank angle greater than 5°, the prosthesis enters late stance. This phase is particularly critical because the contralateral leg is contacting the ground as the prosthesis starts to deliver the positive energy needed to propel the body forward. When the prosthetic foot is lifted from the ground in late stance, the prosthesis enters into swing mode. Swing mode comprises a single phase, controlled using a minimum-jerk trajectory generator. When the prosthesis is again consistently in contact with the ground, it reenters into early stance phase. Similar finite-state machines have been used in previous studies [7], [28], although we used a single state for the entire swing phase.

Walking-Speed Estimation

Walking-speed estimation consists of two steps. First, we obtain an accurate and consistent estimate of the shank orientation in the sagittal plane using a complementary filter [29] to fuse data from the accelerometer and gyroscope located in the prosthetic shank. Then, we derive the

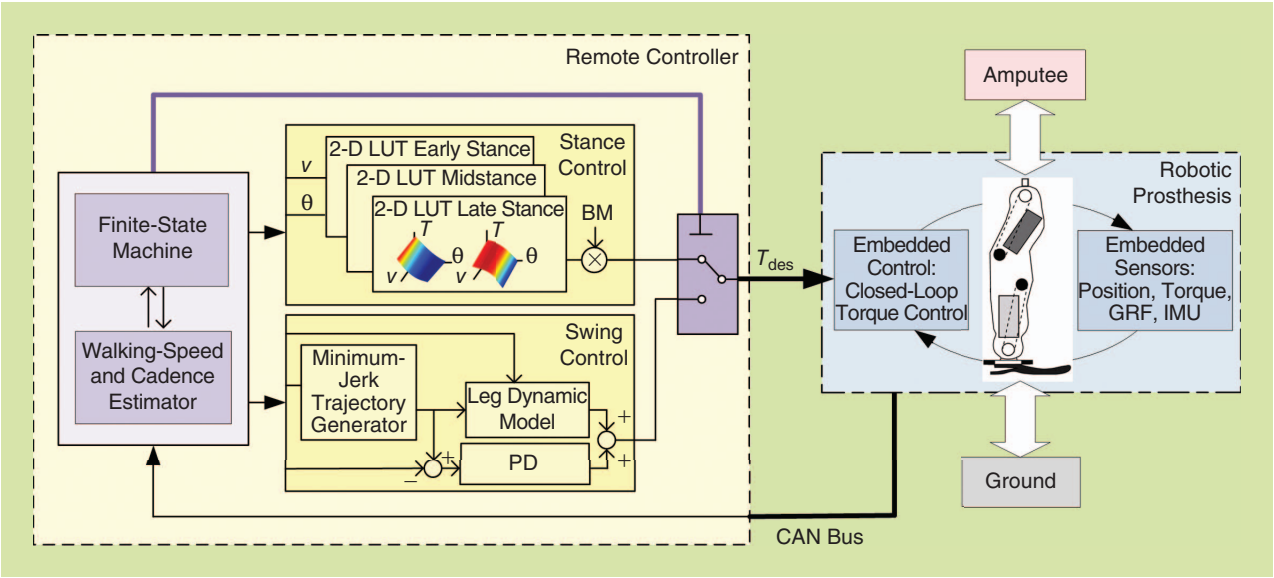

Figure 2. The block diagram of the robotic prosthesis controller. The controller receives input signals from embedded sensors on the prosthesis through a high-speed CAN bus. By combining the prosthesis outputs with the joint angle and GRF, the remote walking-speed estimator computes the forward speed in the sagittal plane (v). At the same time, based on the joint angle, velocity, and GRF, the finite-state machine segments the gait cycle into four parts: early, midstance and late stance and swing phase. For each stance subphase, two 2-D LUTs, implementing normalized able-bodied torque–angle curves for ankle and knee joints, provide the desired torques as a function of current angle (θ), walking speed (v), and patient BM. In the swing phase, a minimum-jerk trajectory generator defines the desired angle for the ankle and knee joints based on the stance-phase duration. The desired joint torques result from the sum of a feed-forward torque command, obtained through a dynamic model of the prosthesis, and a proportional-derivative (PD) closed-loop position control. Finally, the torque references (T_{des}) are transmitted to the closed-loop, low-level, embedded controller on the prosthesis.

thigh and foot orientation using the prosthetic ankle and knee angles. Exploiting a simple three-segment planar model of the leg, we compute the forward velocity of the hip in the sagittal plane using gyroscope data during the stance phase and by integrating accelerometer outputs during the swing phase. As the forward velocity profile has an almost sinusoidal trend with half the duration of the stride [22], we estimate the walking velocity twice during each stride. The first estimate is the average of the forward velocity during the early and midstance phases, which accounts for half of the stride duration. The second estimate is the average during the late stance and swing phase, which accounts for the second half of the stride. The error of the walking-speed estimate on the treadmill has been estimated experimentally to be 8%, in agreement with findings of other researchers using a comparable approach [30]. More accurate walking-speed measurements could be obtained by segmenting the gait cycle in multiple parts, as shown in [31].

Walking Controller

The second stage of the controller is responsible for defining the desired torque profiles to be applied at the ankle and knee joint, based on current estimates of gait phase and walking speed.

In the stance phase, the torque reference for the ankle and knee joint is obtained from intact-leg quasistiffness profiles, as extrapolated from able-bodied studies [22]. In particular, we encoded intact-leg torque–angle curves for two different walking speeds, 0.5 and 1.75 m/s, on bidimensional (2-D) lookup tables (LUTs). Each joint and subphase of stance has

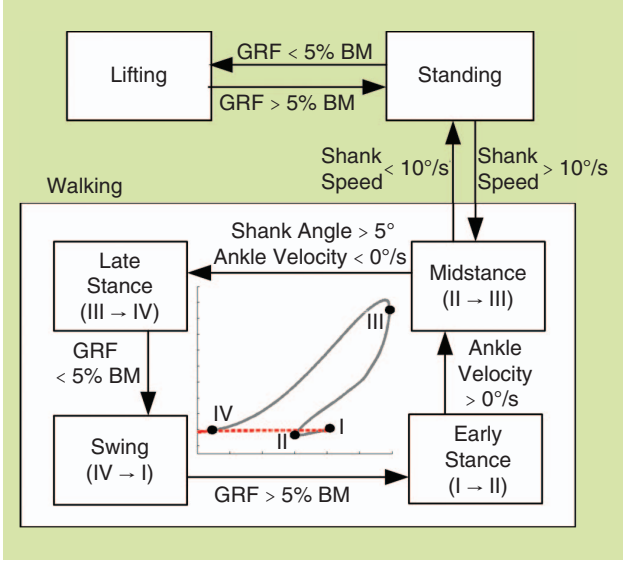

Figure 3. The finite-state machine. Able-bodied ankle quasistiffness is shown in the center of the figure; ideal transitions are indicated with roman numerals (I, II, III, and IV).

a different 2-D LUT that inputs the current joint angle and walking-speed estimate and outputs the desired joint torque normalized by the BM of the patient. A specific torque–angle curve for any possible value of walking speed and angle is then obtained by interpolation. Saturation occurs for input values outside the LUT boundaries. Figure 4 shows the torque–angle curves embedded in the 2-D LUTs for the ankle and knee joints; different colors represent subphases of

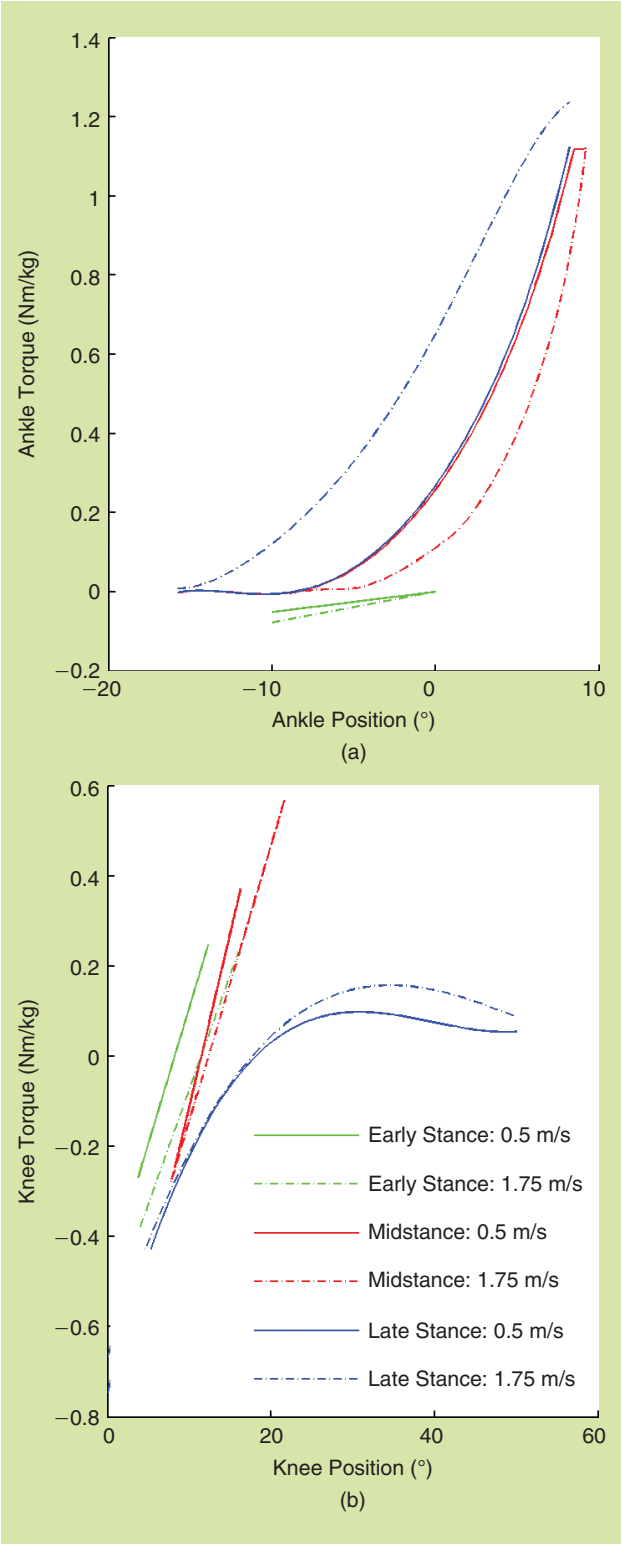

Figure 4. The quasistiffness curves for (a) the ankle and (b) the knee joints as implemented in the 2-D LUTs of the stance controller. Solid lines: low-speed curves. Dashed-dotted lines: high-speed curves. Green: early stance phase. Red: midstance phase. Blue: late stance phase.

stance, and different line styles identify high and low walking speed. The output of each 2-D LUT is multiplied by the subject's BM to define the set-point torque for closed-loop, low-level control. Finally, a low-pass filter is used to smooth the desired torque output during the 10 ms following any transition between different LUT values. Similar approaches based on LUTs have been previously used [32], [33].

In the swing phase, the prosthesis controller enforces a minimum-jerk position trajectory that approximates the behavior of an intact leg at different walking speeds. As the finite-state machine enters into swing mode (i.e., with the prosthetic foot off the ground), the swing-phase controller computes the coefficients of a fifth-order polynomial function that generates the desired minimum-jerk position trajectory. The duration of the swing movement is set to be 0.15 and 0.45 times the previous stance duration for the ankle and knee joint, respectively, based on able-bodied biomechanics [22]. The initial joint angle and velocity of the trajectory are equal to their respective measured values at the end of stance phase. The final joint angle, velocity, and acceleration are fixed to zero for both the ankle and knee joints. Whereas a unique minimum-jerk trajectory is used for the ankle joint, the knee trajectory comprises two parts. The first starts with the knee angle and velocity measured at the last sample of stance phase and ends at the point of maximum knee flexion with zero velocity. The second part starts from the maximum knee flexion and ends with the knee fully extended and zero velocity and acceleration. The acceleration at maximum knee flexion, as well as the starting acceleration of the ankle joint was optimized based on able-bodied data. The maximum knee flexion angle is regulated based on patient anthropometry to ensure an appropriate foot clearance despite the fixed shank length of the prosthesis. The desired angle trajectory is enforced by relying on a strong feedforward torque command (based on the analytical solution of the polynomial function and a dynamic model of the prosthesis) and weaker feedback position control with proportional and derivative terms. Whereas the feedforward command accounts for the inertial, gravitational, and frictional components, the feedback loop reacts to the contingent disturbances that occur during swing phase movement and compensates for possible inaccuracies of the prosthesis dynamic model. The torque references computed by the stance and swing controllers are then enforced through low-level closed-loop control.

Implementation on the Vanderbilt Leg

The proposed control framework has been implemented on a self-contained ankle and knee prosthesis previously developed at Vanderbilt University [14]. This prosthesis is capable of producing biomechanically appropriate torque, power, and range-of-motion at the ankle and knee joints. It is battery operated and uses brushless dc motors controlled by custom servo amplifiers that are integrated into the embedded control system. The embedded control system runs the closed-loop torque controllers for the ankle and knee joint. A remote computer using a hard real-time operative system (xPC target, Mathworks, United States) runs the algorithms that estimate gait-phase and walking speed, as well as the stance phase and swing phase controllers. Communication between the embedded

and remote systems is handled by a high-speed controller area network (CAN) bus (CAN-AC2-PCI, Softing, United States). The embedded controller transmits the local sensing information to the remote system, which processes this information, computes the reference values, and sends them back to the closed-loop controllers. The remote system also stores all measured and processed variables. Communication, processing, and data recording run on the remote control system at the fixed sampling rate of 1 kHz.

Experimental Characterization and Validation

Characterization of the Stance and Swing Controllers with an Able-Bodied Subject

The experimental characterization aimed at assessing the capability of the stance-phase and the swing-phase controllers to regulate the action of the robotic leg in isolation (i.e., independent of walking speed). To this end, an able-bodied subject gave consent to participate in the experiments, which were approved by the Northwestern University Institutional Review Board. The subject walked on the robotic leg using a bypass orthosis at a constant speed, while we manually changed the stance and swing controller parameters to observe how they affected the function of the leg. For each different parameter change tested, the subject walked on the treadmill for 2 min at a constant speed of 0.75 m/s. In the first experiment, we assessed the interpolation of the 2-D LUTs used in the stance phase controller by manually changing the speed input of the 2-D LUTs from their lower (0%) to their upper (100%) boundary in 10% increments. Note that under normal operating conditions, 0–100% would correspond to 0.5–1.75 m/s, although we tested at a constant speed of 0.75 m/s. In the second experiment, we assessed the ability of the swing controller to regulate the desired knee maximum flexion in the swing phase by manually setting the knee flexion angle to 55, 60, 65, or 70°. Finally, we evaluated the regulation of the swing-phase timing by manually setting the swing movement duration to 0.50, 0.75, 1.00, or 1.25 s. For safety reasons, the latter two swing-duration times were tested with a treadmill speed of 0.50 m/s.

Validation of the Proposed Controller with Three Amputee Patients

We evaluated the proposed controllers on three transfemoral amputee patients (see Table 1 for patient characteristics) walking at variable speeds on a treadmill. This experimental protocol was approved by the Northwestern University Institutional Review Board, and participants provided informed consent before the experiment took place. A certified prosthetist fitted the patients with the Vanderbilt robotic prosthesis. The patients' anthropometric measurements were loaded on the prosthesis controller prior to the experiment. The patients familiarized themselves with the prosthesis for about half an hour by performing a series of short walking sessions (fewer than 2 min each) at a constant speed on the treadmill, with at least 2 min of rest between sessions. As the patients' comfort and confidence with the prosthesis improved, we increased the speed of the treadmill, until we identified the highest comfortable speed. After this familiarization phase, we performed three velocity ramps from 0.50 m/s to the highest treadmill speed tested during the familiarization period by manually increasing the speed of the treadmill over approximately 60 s. The patients then repeated the variable-speed test using their prescribed prostheses (Table 1). We added electromechanical goniometers and a foot-switch sensor to the passive prostheses to record the ankle and knee joint angle as well as the timing of ground contact for the heel and toe.

Data Analysis

The prosthesis GRF, torque, angle, and velocity profiles were recorded using the local sensors on the prosthesis. The joint power was calculated during postprocessing. To attenuate the sensor noise for a proper data analysis, we filtered all the data acquired during the experiments offline using a back-and-forth first-order, low-pass Butterworth filter with a cutoff frequency of 10 Hz. The joint torque, power, and work were normalized by dividing by the subject's BM. For each experimental session and each test, we separated the raw data into strides (i.e., the time interval between two consecutive heel strike events on the prosthesis side) using the output of the GRF sensor located on the prosthesis. Within each stride, we computed the maximum and minimum prosthesis angle for the knee and ankle joint as well as the mean walking speed and the duration of stride, stance, and swing phase of the intact and prosthetic leg. In addition, we computed the joint mechanical work for each subphase of stance and overall stance phase by integrating the torque–angle curves, as described in [34]. The first and final three strides for each test were disregarded from the analysis to eliminate non-steady-state walking. Finally, we computed the mean angle, torque, and power profiles for the ankle and knee joint by averaging these variables over all steady-state strides recorded during the constant-speed trials. A similar analysis was performed for the passive prosthesis, except we used the output from the foot-switch sensors to divide the data into strides, and we processed only the ankle and knee joint angle data. All data processing was performed using MATLAB (MathWorks, Natick, Massachusetts, United States).

Results

Characterization of the Controller

In our first experiment, we assessed interpolation capability of the stance-phase controller using 11 manually imposed input-speed values (from zero to 100% of the 2-D LUT's range, in 10% increments). Figure 5 shows the results of the stance-phase controller characterization. For the sake of clarity, we report the ankle quasistiffness profiles recorded in early and midstance [Figure 5(a)] separately from the ones recorded in late stance [Figure 5(b)]. The knee quasistiffness profiles are shown in Figure 5(c). The solid-color lines indicate the averaged profiles; shaded areas represent one standard deviation computed over 30 gait cycles. The

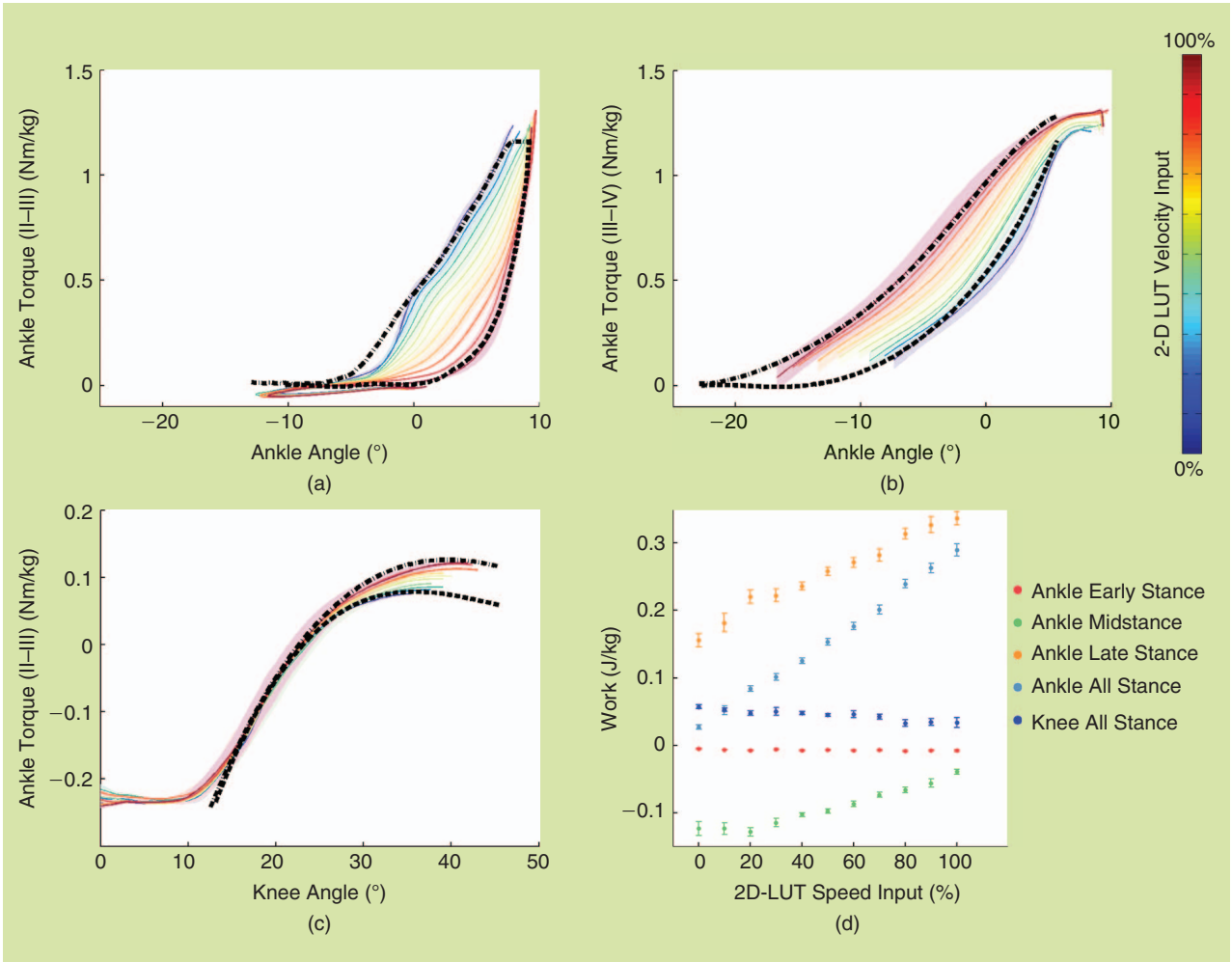

Figure 5. The stance-phase controller characterization: (a)–(c) the quasistiffness profiles for the ankle joint in early and midstance, ankle joint in late stance, and knee joint over all of the stance phases, respectively. Solid lines: average profiles. Shaded areas: ±1 standard deviation. Dashed black lines: quasistiffness curves encoded in the 2-D LUTs. (d) The mechanical work performed by the ankle and knee joints during each subphase of stance and over all of the stance phases.

black lines represent the quasistiffness curves encoded in the 2-D LUTs for the lowest (dashed lines) and highest (dotted-dashed lines) walking speeds, as extracted from able-bodied data [22]. Figure 5(d) shows the mechanical work performed by the prosthesis for the entire stance phase (for the ankle and knee joint) and inside each subphase of stance (for the ankle joint only). Color markers indicate mechanical work averages; error bars represent standard deviations as computed over 30 gait cycles.

As the speed input increased, the measured ankle quasistiffness curves shifted progressively from the bottom (black dashed lines) to the upper (black dotted-dashed lines) boundary of the 2-D LUTs. During midstance [Figure 5(a)], the ankle quasistiffness profile became progressively more nonlinear as the walking speed increased. This increased nonlinearity in turn reduced the braking energy exerted by the ankle during this negative-work phase of the gait cycle [green markers, Figure 5(d)], thus facilitating the inverted pendulum movement at increased walking speed. During late stance [Figure 5(b)], the ankle quasistiffness profile shifted toward a more negative ankle angle at higher walking speeds, increasing the area described by the ankle torque–angle curve during the stance phase, and therefore resulting in greater mechanical work production [orange markers, Figure 5(d)]. As a result of the 2-D LUT interpolation, the net energy at the prosthesis ankle over all of the stance phases [light-blue markers, Figure 5(d)] increased proportionally to the walking-speed input. By fitting the ankle energy measured in the stance phase as a function of the walking-speed input with a first-order polynomial, we obtained a root-mean-square error (RMSE) of 0.004 J/kg and R^2 of 0.9975, with an estimated trend of 0.201 J/kg by m/s.

Similar to the ankle joint, as the speed input increased, the measured knee quasistiffness shifted from the bottom to the upper boundary of the 2-D LUT, resulting in greater extension torque at a higher speed input. The knee work became progressively more negative as the speed input increased [dark blue lines, Figure 5(d)]. However, the effect of speed input on the knee energy was much lower than for the ankle energy. The fitting of the knee energy as a

function of the speed input with a first-order polynomial resulted in an RMSE of 0.003 J/kg and R^2 of 0.898, with an estimated trend of 0.016 J/kg by m/s.

The measured quasistiffness profiles [Figure 5(a)–(c)] for zero and 100% of the speed input (i.e., blue and red lines, respectively) closely matched the quasistiffness curves encoded in the 2-D LUTs (i.e., the upper and lower boundaries of the 2-D LUTs, represented in black dashed and dashed-dotted lines, respectively).

Figure 6 shows the results of the swing characterization experiments. Solid lines represent the average knee swing trajectories, shaded areas indicate one standard deviation, and different trials are plotted using different colors. Figure 6(a) shows the effect of regulating the swing movement duration. Figure 6(b) reports the results for different maximum knee flexion angle settings. Table 2 shows swing duration and maximum knee flexion angle recorded during the tests on the swing controller. The accuracy in controlling the swing duration, defined as the mean difference between the desired duration and recorded duration, was 0.048 s. The precision, evaluated by analyzing the cumulative standard deviation of the swing movement duration over all the trials, was 0.044 s. By repeating the same analysis for the regulation of maximum knee angle, we found an accuracy and precision of 1.04 and 1.10°, respectively. Note that the ankle data were not included in this analysis, as the ankle swing movement duration is significantly shorter than that of the knee [21] and, therefore, not critical for the completion of the swing phase.

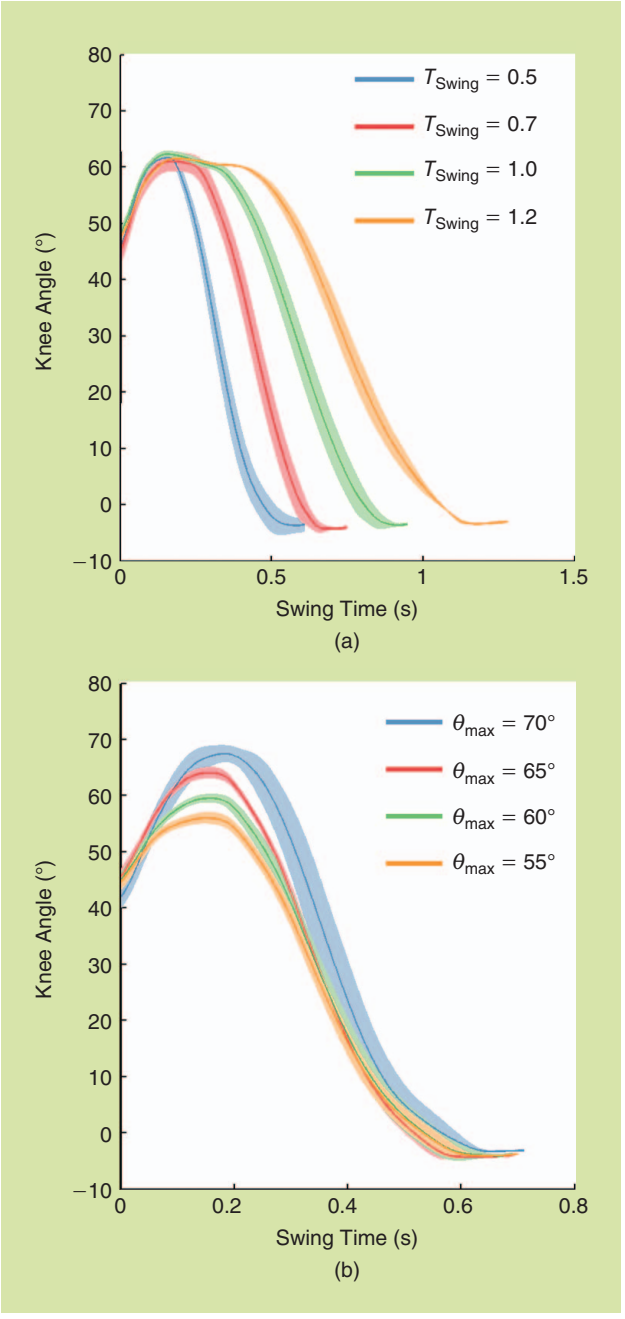

Figure 6. The swing-phase controller characterization. Solid lines: knee swing profiles averaged among all strides completed with the same parameter regulation. Shaded areas: ±1 standard deviation. (a) The results obtained by manually setting the swing duration to 0.5, 0.75, 1, or 1.25 s. (b) The effect of regulating the maximum knee flexion angle to 70, 65, 60, or 55°.

Validation of the Controller

The overall controller, including the walking-speed and cadence estimator, was validated by three amputee patients walking on a treadmill at continuously varying walking speeds with either the robotic leg or their prescribed passive prosthesis. As a representative example, Figure 7 shows the ankle [panels (a) and (b)] and knee [panels (d) and (e)] joint kinematics profiles recorded during the third session performed at variable walking speeds by Patient 1 using the passive prescribed prosthesis and the robotic prosthesis, respectively. Different colors indicate different speeds, as shown by the key on the left side of the figure. Figure 7(c) and (f) shows the measured ankle angle at the transition between midstance to late stance and late stance to swing phase, respectively, superimposed on the equivalent values extracted from able-bodied data (grey-shaded areas) as a function of the walking speed for all amputee patients (shown with different markers and colors).

The finite-state machine performed robustly for all tested speeds and all patients, allowing the correct and timely identification of all gait phase transitions, as can be seen by the joint angle and torque trajectory reported in Figures 7 and 8 for the duration of the experiment. All transitions between different 2-D LUTs in stance phase and from the quasistiffness control in stance phase to the position control in swing phase were very smooth, giving patients comfort and confidence while walking with the robotic prosthesis. Patients had different maximum comfortable speeds as shown in Table 1.

By comparing ankle and knee joint kinematics recoded for the robotic prosthesis and the prescribed, passive prosthesis for Patient 1 (Figure 7), several important differences can be observed. In general, the maximum ankle plantarflexion in early stance and dorsiflexion in midstance were greater for the robotic prosthesis than for the passive prosthesis [Figure 7(a) and (b)]. Given the presumably similar loading conditions in

these two phases of the gait cycle, where the prosthesis is basically absorbing energy, we could then assume that the passive device had greater stiffness than the robotic prosthesis and therefore greater stiffness than an intact leg during walking. Both the maximum ankle dorsiflexion angle in midstance and maximum plantarflexion angle in late stance [Figure 7(a)], increased with walking speed in the robotic prosthesis, in agreement with able-bodied biomechanics [22], [34]. Conversely, the behavior of the passive ankle [Figure 7(a)] remained unaltered.

The robotic prosthesis knee joint [Figure 7(e)] remained locked on the mechanical endstop (located at −2°) from early through midstance, but it resembled intact leg kinematics during late stance and the swing phase. As expected from the swing-controller characterization, the maximum knee flexion angle of the robotic leg in swing phase remained basically unaltered across all tested walking speeds [Figure 7(e)]. For Patient 1, the maximum knee flexion angle ranged between 64.08 and 67.24°, while at the end of the stance phase, the knee angle ranged between 31.4 and 44.9°, the knee velocity between 231.5 and 355.6°/s, and the knee torque between 0.54 and −4.72 Nm. On the other hand, the maximum knee flexion angle of the passive prosthesis increased proportionally with walking speed [Figure 7(d)]. In particular, it started at 55.5° for the slowest walking speed and reached 68.2° for the highest walking speed.

Although patients selected different maximum

Table 2. The results of the swing-controller characterization.

Swing Phase Controller Characterization

Experiment 1—Swing movement duration					
Swing duration (s)	Desired	0.50	0.75	1.00	1.25
	Measured	0.601 ± 0.029	0.747 ± 0.027	0.947 ± 0.037	1.270 ± 0.084
Knee maximum flexion angle (°)	Desired	60	60	60	60
	Measured	60.75 ± 0.84	60.11 ± 1.4	61.12 ± 0.82	60.58 ± 0.19
Experiment 2—Maximum knee flexion angle					
Knee maximum flexion angle (°)	Desired	70	65	60	55
	Measured	68.20 ± 1.5	64.0 ± 1.03	59.5 ± 0.78	56.0 ± 1.07
Swing duration (s)	Desired	0.70	0.70	0.70	0.70
	Measured	0.71 ± 0.04	0.69 ± 0.03	0.69 ± 0.02	0.70 ± 0.05

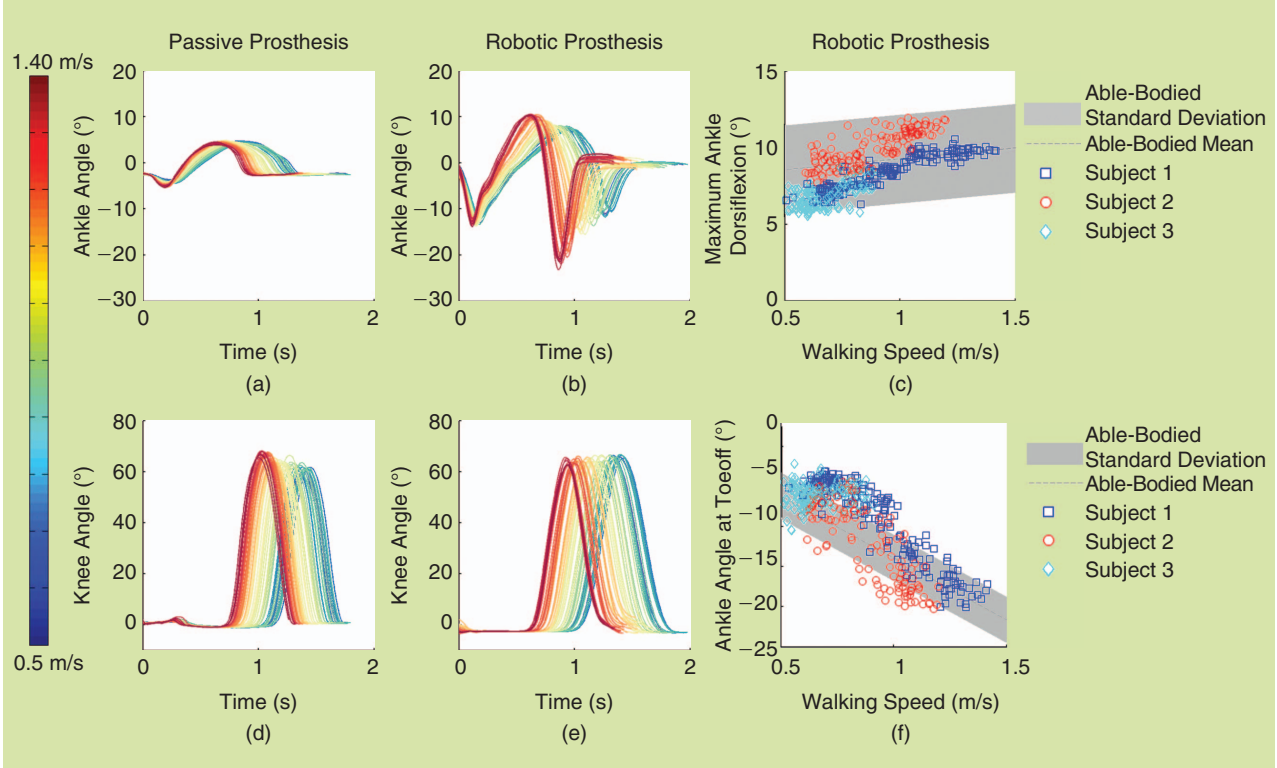

Figure 7. The robotic and passive prosthesis kinematics performance during the variable-walking-speed test. (a) and (b) The ankle angle trajectories and (d) and (e) knee angle trajectories for the robotic and passive prostheses, respectively, as recorded from Patient 1's third session. Time is zeroed at the beginning of each gait cycle, as detected by the finite-state machine entering into early stance phase. (c) and (f) The ankle angle at the transition between midstance to late stance and late stance to swing phase. The grey shaded areas in (c) and (f) indicate equivalent data extracted from able-bodied biomechanics.

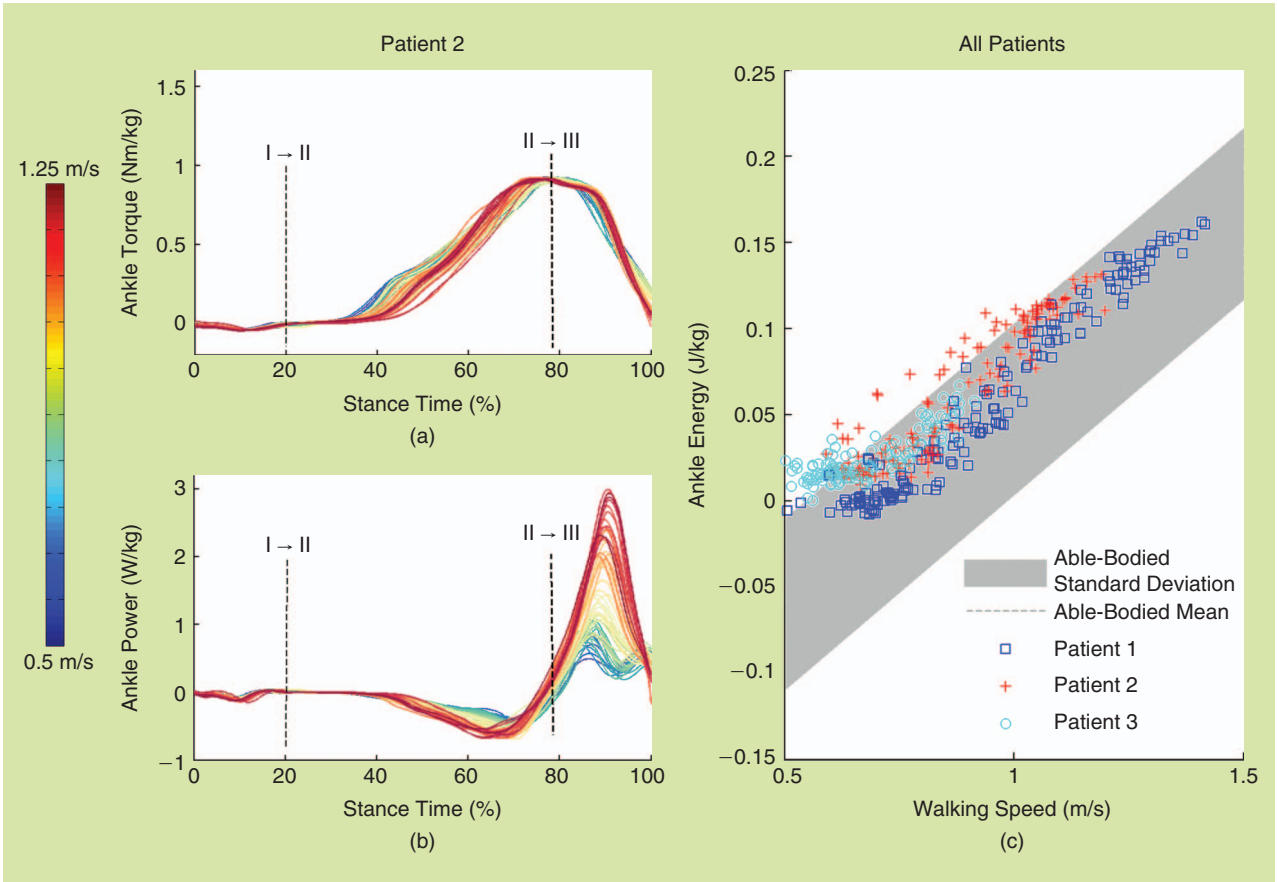

Figure 8. The analysis of ankle energetics during the variable-speed test with the robotic prosthesis. (a) and (b) The ankle-torque and power profiles, respectively, as a function of normalized stance phase time. Vertical shaded lines: transition times from early to midstance (I → II) and midstance to late stance (II → III). Colors: different walking speeds as indicated by the key at left. (c) The ankle energy produced during stance phase as a function of walking speed. The grey shaded areas in (c) indicate equivalent data extracted from able-bodied biomechanics.

speeds, the measured ankle angle at the transition from midstance to late stance [Figure 7(c)] and from late stance to swing phase [Figure 7(f)] approximated to the trend of able-bodied data as a function of walking speeds (grey shaded areas). By fitting the measured ankle angle at toe-off as a function of walking speed with a first-order polynomial function, we obtained an RMSE of 3.05° and R^2 of 0.7154 with a trend of −17.1° by m/s; in comparison, able-bodied experiments reported a trend of −15.5° by m/s and standard deviation of 3.3°. Repeating the same analysis for the ankle dorsiflexion angle at the transition between midstance and late stance resulted instead in an RMSE of 1.51° and R^2 of 0.6425 with a trend of 3.87° by m/s, as opposed to able-bodied data, which show a trend of 1.61° by m/s, and a standard deviation of 2.6°.

Figure 8 presents a detailed analysis of the robotic ankle energetics at varying walking speeds. Figure 8(a) and (b) shows the ankle torque and power profiles, respectively, as a function of the normalized stance time as measured during the third trial of the variable-speed test performed by Patient 2 as a representative example. Figure 8(c) shows the mechanical work performed by the robotic ankle for all patients (with different colors and markers) and all variable-speed test repetitions, superimposed over able-bodied ankle work (grey-shaded area and line) as a function of walking speed.

The ankle torque profile [Figure 8(a)] changed with walking speed, as expected from the results of the stance-controller characterization. As the walking speed increased, (from blue to red lines), the ankle torque profile became progressively steeper both during midstance (I to II) and late stance (II to 100% of stance). It is worth noting that the ankle torque profiles saturated at the transition between midstance to late stance; this was not due to the controller but rather due to hardware limitations imposed by the ankle motor strength of the prosthesis.

The proposed swing controller restored physiological gait symmetry independently of walking speed.

As expected from the overall increase in ankle angular velocity with walking speed, both the negative and positive peak power changed during the experiment [Figure 8(b)]. However, because of quasistiffness modulation as a function of walking speed, the positive power had a much greater increase than the negative power. In particular, the negative peak power ranged between −0.409 W/kg and −0.701 W/kg, whereas the positive

Table 3. The gait symmetry characterization: the root-mean-square difference between prosthesis and intact leg for stride, stance, and swing phase duration.

	Root-Mean-Square Difference (s)		
	Stride	Stance	Swing
Patient 1	0.039	0.043	0.034
Patient 2	0.042	0.056	0.039
Patient 3	0.055	0.089	0.075

peak power ranged between 0.575 W/kg and 2.81 W/kg; a range that is 7.6 times greater than the negative peak power range.

Accordingly, the ankle mechanical work increased proportionally to walking speed [Figure 8(c)]. A linear fitting with a first-order polynomial on all patients and test repetitions estimated an energy increase rate of 0.194 J/kg by m/s with an RMSE of 0.018 J/kg and R^2 of 0.8859. This result closely matches the rate of ankle energy increase that we obtained in stance-control characterization (i.e., 0.201 J/kg by m/s), though this was performed at a constant walking speed. Most importantly, the measured ankle work matched the values observed in able-bodied persons, which equals 0.214 J/kg by m/s [shaded-grey areas, Figure 8(c)] across all tested walking speeds.

Figure 9 and Table 3 present the analysis of gait symmetry during the variable-speed test. Figure 9(a) shows the duration of stride, stance phase, and swing phase for both the robotic prosthesis and intact leg for each step measured on the third session of the variable-speed test by Patient 3. Figure 9(b) shows the average duration of stance and swing phase, normalized by stride duration for all three patients for both the robotic prosthesis and intact leg. Table 3 shows the root-mean-square difference between the duration of stride, stance phase, and swing phase for the robotic prosthesis and intact leg, for all amputee patients.

As shown by Patient 3 in Figure 9(a), as the variable-speed test progressed, stride, stance phase, and swing phase duration decreased, indicating an increase in gait cadence. Note that the robotic prosthesis and intact leg showed a good temporal symmetry. The root-mean-square difference between the prosthesis and intact leg (Table 3) ranged between 0.039 and 0.089 s. In addition, the proportion of stance and swing duration inside the gait cycle was very similar for the robotic prosthesis and intact leg across all variable test durations [Figure 9(b)].

Discussion

Robotic prostheses can restore physiological walking ability in individuals with transfemoral amputations. However, available control strategies require subject-specific tuning to provide biologically accurate torques at a specific walking speed.

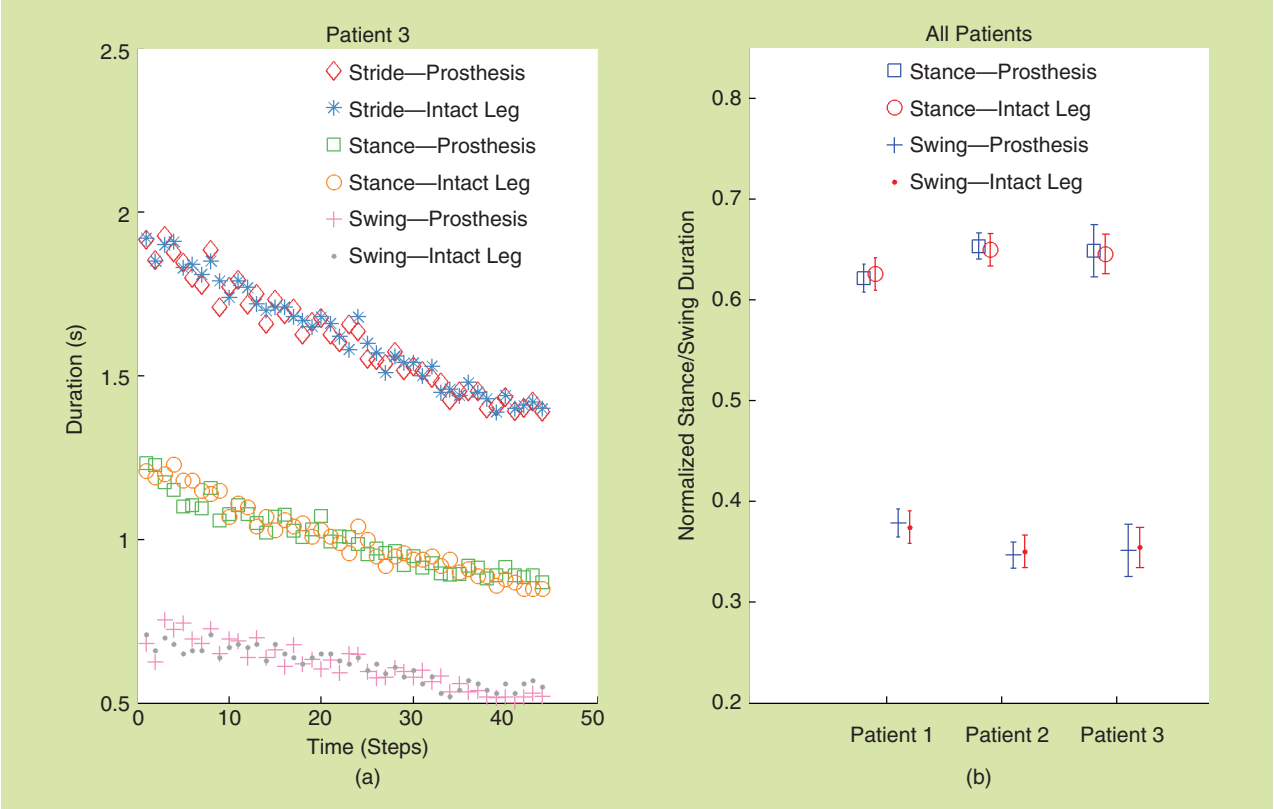

Figure 9. The analysis of gait symmetry during the variable-speed test with the robotic prosthesis: (a) the duration of stride, stance phase, and swing phase for both the robotic prosthesis and intact leg as measured at each step during the third iteration of the variable-speed test performed by Patient 3, as a representative example, and (b) the normalized duration of stance and swing phase for the prosthesis (blue) and the intact leg (red) for all patients and all repetitions of the variable-speed test.

At different walking speeds, the action of the prosthesis is not optimal because joint speeds (and tuned joint impedance) do not linearly correspond to walking speed, forcing amputees to rely on costly compensatory strategies. To reach the full potential of robotic prostheses, there is the need to develop a controller that can provide biologically accurate torques across a wide range of walking speeds without requiring speed-specific prosthesis tuning. Toward this goal, we developed a new control framework that automatically adapts prosthesis action to walking speed based on able-bodied biomechanics. Preliminary validation in three transfemoral amputee patients showed that the proposed controller could restore physiological gait energetics and symmetry across all speeds without tuning—only patients' BM and height were input into the controller before the experiments.

The primary goal of the tests performed with the able-bodied subject was to characterize how the stance and swing controllers responded to different parameter regulations independently of walking speed. The first test assessed the ability of the stance phase controller to obtain a desired quasistiffness curve independently of joint velocity, which varies for each subject when walking at the same speed and cadence. The measured quasistiffness for the highest- and lowest-speed inputs closely matched the two quasistiffness curves encoded in the 2-D LUTs, showing that the accuracy and responsiveness of the low-level prosthesis controller was appropriate to virtually enforce the intact-leg quasistiffness during walking. In addition, the interpolation of the two quasistiffness curves encoded in each 2-D LUT for the upper and lower boundaries of the walking-speed input allowed the modulation of the shape of the ankle and knee quasistiffness curves as a function of walking-speed input, in agreement with able-bodied studies in [22] and [34]. The measured ankle and knee energetics quantitatively matched able-bodied values [6], [34], thus demonstrating the ability of the proposed controller to replicate intact leg energetics through the interpolation of intact leg quasistiffness profiles. Cumulatively, the results of this test prove that enforcing quasistiffness profiles allows modulation of ankle mechanical work independently of the actual joint speed, which is necessary to achieve effective walking-speed adaptation without subject- or speed-specific tuning.

The swing characterization experiment assessed the ability to regulate maximum knee flexion and swing movement duration independently of initial swing conditions (i.e., joint angle, velocity, and torque) that vary due to a different regulation of the stance controller, a different walking speed, or a different walking pattern. The measured accuracy and precision of the swing movement were well within able-bodied movement variability [22], thus satisfying a primary requirement for the proposed swing controller. Importantly, the regulation of the swing duration and maximum knee flexion angle are independent of one another (Figure 7). This provides a notable advantage of the proposed control approach over an impedance-based strategy, as it allowed us to decrease the swing time proportionally to the stance time without worrying about foot clearance. The results of this test prove that the proposed controller can consistently modulate the range of motion and duration of swing movement independently of stance phase control, which is necessary to produce physiological prosthesis swing at different walking speeds.

Three transfemoral amputee patients tested the proposed controllers by walking on a treadmill at a continuously variable speed. Analysis of the robotic prosthesis kinematics (Figure 7) highlights the ability of the proposed control framework to fairly approximate the biomechanical behavior of intact legs at different walking speeds. However, the robotic prosthesis lacked stance knee flexion (i.e., the prosthesis knee joint remained fully extended in early and midstance). This phenomenon has been previously attributed to the patients' tendency to exaggerate hip extension during the weight acceptance phase, together with the compliance of the human thigh at the interface with the prosthesis socket [14]. Our results confirm these observations, although exploring this phenomenon was not a focus of this study. Prosthesis ankle kinematics changed with walking speed as a result of quasistiffness modulation. Ankle maximum dorsiflexion and plantarflexion angle (Figure 7) in the stance phase followed the trend observed on able-bodied subjects [22], [34], [35] for all patients, suggesting that the stance controller adequately adapted joint torque to walking speed, despite the ankle torque saturation occurring at the transition between midstance to late stance (Figure 8). The measured kinematics variability was also very close to able-bodied variability, which is interesting as it has been previously observed that amputees tend to have higher variability in walking. These results suggest that the proposed quasistiffness-based controller promoted a natural dynamic interaction of patients with the prosthesis at different speeds.

By modulating quasistiffness based on walking speed, we achieved physiological prosthesis energetics for all patients without the need for tuning.

The adaptation of quasistiffness with walking speed resulted in a nonlinear modulation of joint torque inside the gait cycle (Figure 8). The modulation of temporal torque profiles in turn increased both the negative and positive power peaks with walking speed. However, in agreement with several able-bodied studies [22], [34], [35], the positive power increased more than the negative power. Most importantly, by modulating quasistiffness based on walking speed, we achieved physiological prosthesis energetics for all patients without the need for tuning. This is particularly important because providing physiological energy reduced the metabolic cost of walking in a powered ankle–foot prostheses [6]. Robotic transfemoral prosthesis able to provide physiological energetics might also reduce the metabolic cost of walking.

As expected from the swing controller characterization, the maximum knee flexion angle in the swing phase remained unaltered at different walking speeds. This result is particularly significant if we consider the high variability of the swing starting conditions in terms of torque, angle, and velocity. On the other hand, passive prosthetic knees were unable to entirely compensate for the variation of the inertial torque following the change in walking speed, as shown by the variation of knee maximum flexion angle. Unlike passive prostheses, the proposed controller allowed a biomimetic swing trajectory at any walking speed [22].

The analysis of the stride, stance, and swing phase durations shows that the proposed swing controller restored physiological gait symmetry independently of walking speed. This result is significant because the effective swing phase duration depends not only on swing movement duration, but also on the volition of the patient. If patients had waited too long at the end of the swing movement before loading their body weight on the prosthesis, physiological gait symmetry would have not been achieved. Our results show not only that swing movement duration was properly adapted at each step but also that patients trusted the variable cadence control and moved in synchrony with the robotic prosthesis.

The time needed to tune a powered transfemoral prosthesis for each patient has been identified as a main obstacle to their clinical viability [36]. Our control framework can provide physiological function without any need for tuning; we only had to input patient's BM and height into the controller. All patients could walk comfortably with the prosthesis at varying speeds after minimal training—about 15 min of walking practice—with no tuning. This result encourages us to test the proposed controller on a larger population, focusing on clinical outcomes.

A limitation of this article is the lack of a direct comparison with previously proposed powered prostheses and control methods. Nonetheless, the goal of this article was to thoroughly assess the control performance of the proposed framework and to obtain a preliminary validation on a limited sample size that could justify a larger clinically oriented study. Future work will aim to assess the clinical benefits of the proposed approach in comparison to other powered prostheses and control methods. Future studies will need to include a larger sample size to properly verify the ability of the proposed controller to generalize across different individuals. In addition, further insights could be gained through additional outcome measurements, for example, by recording kinematics, kinetics, and electromyography signals from the residual limb and contralateral leg. Moreover, heart rate and metabolic consumption measurements would be desirable to verify possible systemic benefits.

Conclusions

Providing positive net energy over the gait cycle is one of the biggest advantages of powered prostheses over passive devices [26], [37]. Positive net energy is needed to walk on level ground at moderate to high speeds [11], [38], to properly propel and support the body [39], and to accelerate the leg into swing [40], [41]. However, the amount of positive net energy required depends on walking speed, which imposes a complex, nonlinear modulation of torque [42]. For the first time, the proposed stance phase controller enabled a transfemoral prosthesis to restore physiological gait energetics over a wide range of walking speeds without any subject- or speed-specific tuning by relying on able-bodied intact leg quasistiffness profiles. In addition, the proposed swing controller enabled the robotic prosthesis to provide a smooth swing movement that drove the prosthetic leg through a physiologically appropriate trajectory independently of the stance-phase controller. By timing the swing movement based on the duration of the previous stance phase, the robotic prosthesis was able to restore physiological gait symmetry, which is fundamental to restore natural gait stability and efficiency to persons with transfemoral amputations [43]. Future work will be dedicated to embedding the controller onto the onboard electronics of the prosthesis and evaluating its performance in a larger clinical population, to assess improvements in walking stability and metabolic efficiency compared to passive prostheses and powered prostheses using other control approaches.

Acknowledgment

We would like to thank Suzanne Finucane, Elizabeth Halsne, and Rudhram Gajendran for their help with the experimental setup and data acquisition.

References

[1] K. Ziegler-Graham, E. J. MacKenzie, P. L. Ephraim, T. G. Travison, and R. Brookmeyer, "Estimating the prevalence of limb loss in the United States: 2005 to 2050," *Arch. Phys. Med. Rehab.*, vol. 89, no. 3, pp. 422–429, 2008.

[2] R. L. Waters, J. Perry, D. Antonelli, and H. Hislop, "Energy cost of walking of amputees: The influence of level of amputation," *J. Bone Joint Surg. Amer.*, vol. 58, no. 1, pp. 42–46, Jan. 1976.

[3] J. P. Pell, P. T. Donnan, F. G. Fowkes, and C. V. Ruckley, "Quality of life following lower limb amputation for peripheral arterial disease," *Eur. J. Vasc. Surg.*, vol. 7, no. 4, pp. 448–451, 1993.

[4] H. Sadeghi, P. Allard, and M. Duhaime, "Muscle power compensatory mechanisms in below-knee amputee gait," *Amer. J. Phys. Med. Rehab.*, vol. 80, pp. 25–32, Jan. 2001.

[5] R. Seroussi and A. Gitter, "Mechanical work adaptations of above-knee amputee ambulation," *Arch. Phys. Med. Rehab.*, vol. 77, pp. 1209–1214, Nov. 1996.

[6] H. M. Herr and A. M. Grabowski, "Bionic ankle-foot prosthesis normalizes walking gait for persons with leg amputation," *Proc. Biol. Sci.*, vol. 279, no. 1728, pp. 457–464, Feb. 2012.

[7] S. K. Au, J. Weber, and H. Herr, "Powered ankle–foot prosthesis improves walking metabolic economy," *IEEE Trans. Robot.*, vol. 25, no. 1, pp. 51–66, Feb. 2009.

[8] P. Cherelle, V. Grosu, A. Matthys, B. Vanderborght, and D. Lefeber, "Design and validation of the ankle mimicking prosthetic foot 2.0.," *IEEE Trans. Neural Syst. Rehab. Eng.*, vol. 22, no. 1, pp. 138–148, Oct. 2013.

[9] J. K. Hitt, T. G. Sugar, M. Holgate, and R. Bellman, "An active foot-ankle prosthesis with biomechanical energy regeneration," *J. Med. Device*, vol. 4, no. 1, p. 011003, 2010.

[10] D. A. Winter, "Energy generation and absorption at the ankle and knee during fast, natural, and slow cadences," *Clin. Orthop. Relat. Res.*, vol. 175, pp. 147–154, May 1983.
[11] J. M. Donelan, R. Kram, and A. D. Kuo, "Mechanical work for step-to-step transitions is a major determinant of the metabolic cost of human walking," *J. Exp. Biol.*, vol. 205, pt. 23, pp. 3717–3127, Dec. 2002.
[12] R. R. Neptune, S. A. Kautz, and F. E. Zajac, "Contributions of the individual ankle plantar flexors to support, forward progression and swing initiation during walking," *J. Biomech.*, vol. 34, no. 11, pp. 1387–1398, Nov. 2001.
[13] J. Doke, J. M. Donelan, and A. D. Kuo, "Mechanics and energetics of swinging the human leg," *J. Exp. Biol.*, vol. 208, pt. 3, pp. 439–445, Feb. 2005.
[14] F. Sup, A. Bohara, and M. Goldfarb, "Design and control of a powered transfemoral prosthesis," *Int. J. Robot. Res.*, vol. 27, no. 2, pp. 263–273, Feb. 2008.
[15] A. M. Simon, N. P. Fey, S. B. Finucane, R. D. Lipschutz, and L. J. Hargrove, "Strategies to reduce the configuration time for a powered knee and ankle prosthesis across multiple ambulation modes," in *Proc. IEEE Int. Conf. Rehabilitation Robotics*, June 2013, pp. 1–6.
[16] M. A. Holgate, W. B. Alexander, and T. G. Sugar, "Control algorithms for ankle robots: A reflection on the state-of-the-art and presentation of two novel algorithms," in *Proc. BioRob 2nd IEEE RAS EMBS Int. Conf. Biomedical Robotics Biomechatronics*, 2008, pp. 97–102.
[17] R. D. Gregg and J. W. Sensinger, "Towards biomimetic virtual constraint control of a powered prosthetic leg," *IEEE Trans. Control Syst. Technol.*, vol. 22, no. 1, pp. 246–254, Jan. 2014.
[18] R. D. Gregg, T. Lenzi, L. J. Hargrove, and J. W. Sensinger, "Virtual constraint control of a powered prosthetic leg: From simulation to experiments with transfemoral amputees," *IEEE Trans. Robot.*, to be published.
[19] R. D. Gregg, T. Lenzi, N. P. Fey, L. J. Hargrove, and J. W. Sensinger, "Experimental effective shape control of a powered transfemoral prosthesis," in *Proc. IEEE Int. Conf. Rehabilitation Robotics*, June 2013, pp. 1–7.
[20] E. J. Rouse, R. D. Gregg, L. J. Hargrove, and J. W. Sensinger, "The difference between stiffness and quasistiffness in the context of biomechanical modeling," *IEEE Trans. Biomed. Eng.*, vol. 60, no. 2, pp. 562–568, Feb. 2013.
[21] R. Davis and P. DeLuca, "Gait characterization via dynamic joint stiffness," *Gait Posture*, vol. 4, no. 3, pp. 224–231, 1996.
[22] D. A. Winter, *Biomechanics and Motor Control of Human Movement*, 2nd ed. New York: Wiley, 1990, p. 277.
[23] K. Shamaei, G. S. Sawicki, and A. M. Dollar, "Estimation of quasistiffness of the human knee in the stance phase of walking," *PLoS One*, vol. 8, no. 3, p. e59993, Jan. 2013.
[24] K. Shamaei, G. S. Sawicki, and A. M. Dollar, "Estimation of quasistiffness and propulsive work of the human ankle in the stance phase of walking," *PLoS One*, vol. 8, no. 3, p. e59935, Jan. 2013.
[25] D. A. Winter and D. G. E. Robertson, "Joint torque and energy patterns in normal gait," *Biol. Cybern.*, vol. 29, no. 3, pp. 137–142, 1978.
[26] S. Au and H. Herr, "Powered ankle-foot prosthesis," *IEEE Robot. Automat. Mag.*, vol. 15, no. 3, pp. 52–59, Sept. 2008.
[27] H. Vallery, J. Veneman, E. van Asseldonk, R. Ekkelenkamp, M. Buss, and H. van Der Kooij, "Compliant actuation of rehabilitation robots," *IEEE Robot. Automat. Mag.*, vol. 15, no. 3, pp. 60–69, Sept. 2008.
[28] F. Sup, H. A. Varol, J. Mitchell, T. J. Withrow, and M. Goldfarb, "Self-contained powered knee and ankle prosthesis: Initial evaluation on a transfemoral amputee," in *Proc. IEEE Int. Conf. Rehabilitation Robotics*, June 2009, pp. 638–644.
[29] R. Mahony, S. Member, T. Hamel, and J. Pflimlin, "Nonlinear complementary filters on the special orthogonal group," *IEEE Trans. Autom. Control*, vol. 53, no. 5, pp. 1203–1218, 2008.
[30] S. Yang and Q. Li, "Inertial sensor-based methods in walking speed estimation: A systematic review," *Sensors*, vol. 12, no. 5, pp. 6102–6116, Jan. 2012.
[31] R. R. Torrealba, J. Cappelletto, L. Fermín-León, J. C. Grieco, and G. Fernández-López, "Statistics-based technique for automated detection of gait events from accelerometer signals," *Electron. Lett.*, vol. 46, no. 22, p. 1483, 2010.
[32] M. A. Holgate, T. G. Sugar, and W. B. Alexander, "A novel control algorithm for wearable robotics using phase plane invariants," in *Proc. IEEE Int. Conf. Robotics Automation*, 2009, pp. 3845–3850.
[33] T. Lenzi, M. C. Carrozza, and S. K. Agrawal, "Powered hip exoskeletons can reduce the user's hip and ankle muscle activations during walking," *IEEE Trans. Neural Syst. Rehab. Eng.*, vol. 21, no. 6, pp. 938–948, Nov. 2013.
[34] A. H. Hansen, D. S. Childress, S. C. Miff, S. A. Gard, and K. P. Mesplay, "The human ankle during walking: Implications for design of biomimetic ankle prostheses," *J. Biomech.*, vol. 37, no. 10, pp. 1467–1474, 2004.
[35] M. L. Palmer, "Sagittal plane characterization of normal human ankle function across a range of walking speeds," M.S. thesis Mech. Eng., Massachusetts Inst. Technology, Cambridge, MA, 2002.
[36] A. M. Simon, K. A. Ingraham, N. P. Fey, S. B. Finucane, R. D. Lipschutz, A. J. Young, and L. J. Hargrove, "Configuring a powered knee and ankle prosthesis for transfemoral amputees within five specific ambulation modes," *PLoS One*, vol. 9, no. 6, p. e99387, Jan. 2014.
[37] R. Seroussi and A. Gitter, "Mechanical work adaptations of above-knee amputee ambulation," *Arch. Phys. Med. Rehab.*, vol. 77, no. 11, pp. 1209–1214, Nov. 1996.
[38] S. H. Collins and A. D. Kuo, "Recycling energy to restore impaired ankle function during human walking," *PLoS One*, vol. 5, no. 2, p. e9307, Jan. 2010.
[39] J. L. Johansson, D. M. Sherrill, P. O. Riley, P. Bonato, and H. Herr, "A clinical comparison of variable-damping and mechanically passive prosthetic knee devices," *Amer. J. Phys. Med. Rehab.*, vol. 84, no. 8, pp. 563–575, Aug. 2005.
[40] R. J. Zmitrewicz, R. R. Neptune, and K. Sasaki, "Mechanical energetic contributions from individual muscles and elastic prosthetic feet during symmetric unilateral transtibial amputee walking: A theoretical study," *J. Biomech.*, vol. 40, no. 8, pp. 1824–1831, Jan. 2007.
[41] M. Q. Liu, F. C. Anderson, M. H. Schwartz, and S. L. Delp, "Muscle contributions to support and progression over a range of walking speeds," *J. Biomech.*, vol. 41, no. 15, pp. 3243–3252, Nov. 2008.
[42] D. A. Winter, "Energy generation and absorption at the ankle and knee during fast, natural, and slow cadences," *Clin. Orthop. Relat. Res.*, vol. 175, pp. 147–154, May 1983.
[43] L. Nolan, A. Wit, K. Dudziński, A. Lees, M. Lake, and M. Wychowański, "Adjustments in gait symmetry with walking speed in trans-femoral and trans-tibial amputees," *Gait Posture*, vol. 17, no. 2, pp. 142–151, Apr. 2003.

Tommaso Lenzi, Rehabilitation Institute of Chicago, Chicago, Illinois, United States. E-mail: lenzi@ieee.org.

Levi J. Hargrove, Rehabilitation Institute of Chicago, Chicago, Illinois, United States. E-mail: l-hargrove@northwestern.edu.

Jonathon W. Sensinger, University of New Brunswick, Fredericton, New Brunswick, Canada. E-mail: sensinger@ieee.org.